Evidence of weak superconductivity at the room-temperature grown LaAlO$_3$/SrTiO$_3$ interface

G. E. D. K. Prawiroatmodjo,[1,*] F. Trier,[2] D. V. Christensen,[2] Y. Chen,[2] N. Pryds,[2] and T. S. Jespersen[1]

[1]*Center for Quantum Devices, Niels Bohr Institute, University of Copenhagen, Universitetsparken 5, 2100 Copenhagen, Denmark*
[2]*Department of Energy Conversion and Storage, Technical University of Denmark, Risø Campus, 4000 Roskilde, Denmark*

The two-dimensional electron gas at the crystalline LaAlO$_3$/SrTiO$_3$ (*c*-LAO/STO) interface has sparked large interest due to its exotic properties, including an intriguing gate-tunable superconducting phase. While there is growing evidence of pronounced spatial inhomogeneity in the conductivity at STO-based interfaces, the consequences for superconductivity remain largely unknown. We study interfaces based on amorphous LAO top layers grown at room temperature (*a*-LAO/STO) and demonstrate a superconducting phase similar to *c*-LAO/STO, however, with a gate-tunable critical temperature of 460 mK. The dependence of the superconducting critical current on temperature, magnetic field, and back-gate-controlled doping is found to be consistently described by a model of a random array of Josephson-coupled superconducting domains.

Understanding the physics of normal/superconductor hybrid systems has been a subject of active research since the original work of Josephson [1]. Recently, however, driven by theoretical insights [2,3] and experimentally enabled by the development of new materials, nanoscale hybrid devices have led to a number of key breakthroughs in quantum transport [4–6]. Strontium titanate (STO) is a wide-gap insulating perovskite oxide with a strong interdependence of structural, magnetic, and electronic properties [7,8]. Interfacing STO with other complex oxides, such as lanthanum aluminate (LAO), leads to a two-dimensional electron gas with remarkable properties, such as high mobility [9] and gate-tunable superconductivity [10,11] coexisting with magnetism [12,13] and strong spin-orbit coupling [14]. This system therefore provides the right conditions for creating exotic quantum states in a new generation of hybrid devices with electrostatic control [15]. In order to exploit this potential, however, a detailed understanding of the nature of the superconducting phase and how it is affected by nearby electrostatic gates is required, and methods are needed for fabricating advanced device geometries.

Recently, the importance of micron scale inhomogeneity for the properties of the two-dimensional electron system in STO-based heterostructures has become evident from direct spatial mapping of the current distribution, the superfluid density, and the electrostatic landscape [12,16,17]. Furthermore, signs of phase-coherent superconductivity in the metallic and insulating states were found [18–20] and attributed to tetragonal domain boundaries in STO. The superconducting transition is commonly described as a two-dimensional system using the Berezinskii-Kosterlitz-Thouless (BKT) model [10,11,21,22], valid for homogeneous or granular superconducting thin films [23], however, an alternative model based on the percolation of superconducting islands embedded in a metallic background is also found to provide a consistent description [24–26]. So far, the possible consequences of inhomogeneity on the critical current and its dependence on magnetic field, temperature, and electrostatic doping have not yet been considered.
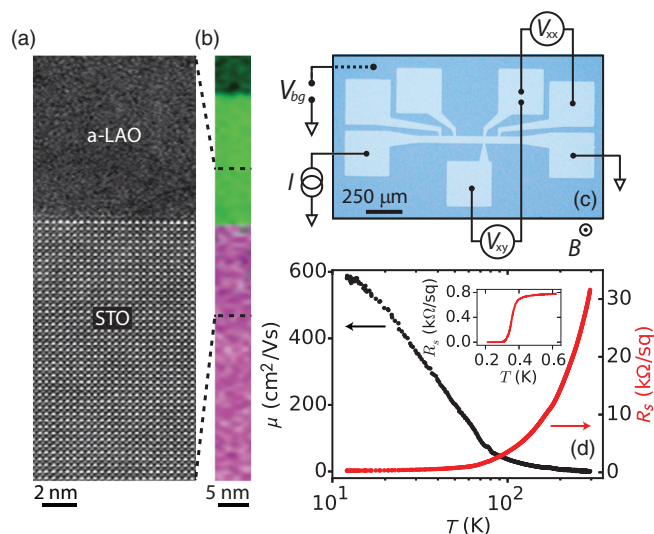
—————
*guen@nbi.dk

FIG. 1. (a) HAADF and (b) EELS (La is green and Ti is purple) STEM images showing the amorphous-LAO/STO interface. (c) Optical micrograph of the Hall bar device. The magnetic field B is applied perpendicular to the chip plane and the gate voltage V_{bg} is varied to tune the electrostatic doping of the device. (d) Mobility μ and sheet resistance R_s as a function of the temperature T. The superconducting transition at $T = 360$ mK at $V_{bg} = 0$ V is shown in the inset.

The aim of the present paper is twofold. First, we introduce interfaces of STO and room-temperature grown amorphous LAO (*a*-LAO) [27–29] to the family of STO-based heterostructures that exhibit superconductivity. While the doping mechanism leading to conductivity in *a*-LAO/STO is dominated by oxygen vacancies [27–29] different from polar discontinuities in *c*-LAO/STO, the characteristics of superconductivity are found to be similar [10,11]. However, we find that *a*-LAO/STO exhibits a significantly higher T_c than reported for *c*-LAO/STO and has the added benefit that room-temperature growth is compatible with standard semiconductor fabrication processes [29]. We include a full phase diagram of the critical current dependence on temperature and magnetic field. Second, we study and compare the gate dependence of the superconducting critical current $I_c(V_{bg})$ and critical

temperature $T_c(V_{bg})$. Both exhibit a domelike dependence on V_{bg}, however, with a clear shift which provides qualitative evidence a superconducting phase best described as a random array of superconducting domains [24] interconnected by metallic weak links or Josephson junctions (JJs) [30]. Such Josephson junction arrays (JJAs) have been shown to undergo a BKT quantum phase transition [21,22,31], consistent with previous work on *c*-LAO/STO [10,11]. The presence of intrinsic weakly coupled superconducting domains may be a crucial element in the design and study of gate-defined devices at STO-based interfaces [32].

Our samples were grown by room-temperature pulsed laser deposition (PLD) and patterned in a Hall bar geometry (width $W = 50\ \mu$m, length $L = 100\ \mu$m) using a LaSrMnO$_3$ hard mask following Ref. [33]. The 16 nm LAO top layer is amorphous [34], as confirmed by the absence of long-range order in the cross-sectional high-angle annular dark-field (HAADF) scanning transmission electron microscopy (STEM) image and corresponding electron energy loss spectroscopy (EELS) scan in Figs. 1(a) and 1(b) of an unpatterned reference sample. Figure 1(c) shows an optical image of the final device. The chip was glued to a ceramic chip carrier using conducting silver paste and the back plane of the chip served as a global electrostatic back gate, tuning the interface carrier density when biased at a voltage V_{bg}.

Initial characterization of the device was done by sourcing a current I and measuring the longitudinal and transverse voltages V_{xx} and V_{xy} while applying an out-of-plane magnetic field B [Fig. 1(c)]. The temperature dependence of the sheet resistance $R_s = V_{xx}W/LI$ is shown in Fig. 1(d), confirming the metallic behavior of the sample and the carrier density $n_s = 1/eR_H$ is found from the measured Hall coefficient $R_H = |\partial R_{xy}/\partial B|_{B=0\ \mathrm{T}}$. Upon cooling the sample from room temperature, n_s is constant at 0.4×10^{14} cm^{-2} until $T = 90$ K from where it linearly decreases to a value of 0.2×10^{14} cm^{-2} at 10 K. The carrier freeze-out below ${\sim}100$ K is consistent with previous reports on both amorphous and crystalline LAO/STO samples [28,35,36]. The mobility $\mu_H = 1/n_s eR_s$ [Fig. 1(d)] increases upon cooling and reaches a value of ${\sim}600$ cm^2/V s at low temperature. Subsequently, the sample was measured in a dilution refrigerator with a base temperature of 22 mK. A transition to the superconducting state is observed at $T_c = 360$ mK [inset to Fig. 1(d)]. Here, the critical temperature T_c was defined as the temperature where R_s is 50% of the normal-state resistance R_N at $T = 600$ mK. The transition temperature is comparable to the values ranging from 200 to 300 mK reported for *c*-LAO/STO samples [10,11,18,37].

To study the properties of the superconducting phase, T_c was measured at different B, sweeping the temperature at a slow 2 mK/min temperature ramp rate to ensure a stable equilibrium situation. Figure 2(a) shows $R_s(T)$ for different magnetic fields and the resulting $T_c(B)$ is shown in Fig. 2(b). Also included in Fig. 2(b) is T_c extracted from fitting the $B = 0$ T data to the effective medium theory (EMT) of Ref. [24], which considers a sample composed of percolating superconducting regions with a Gaussian distribution of transition temperatures with width γ and average $\bar{T}_c$. The fit shown by the dashed line in Fig. 2(a) is in good agreement with the experimental curve [38]. The 50% transition point (reached at $T = \bar{T}_c$) agrees with the T_c found by fitting EMT theory
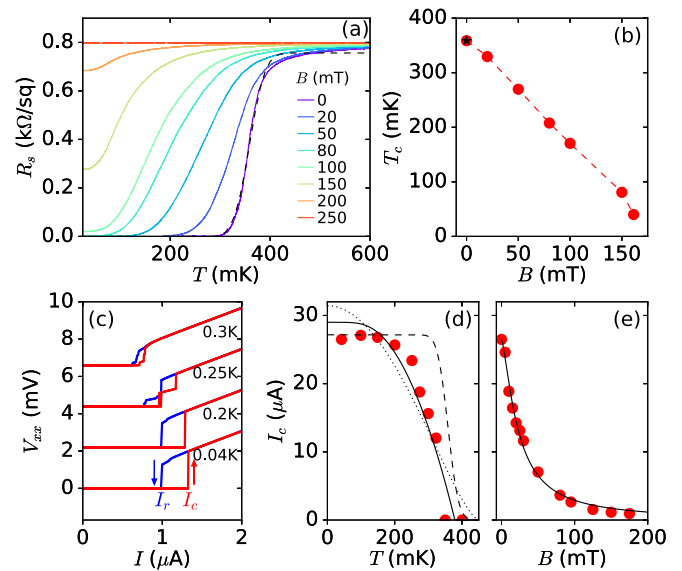

FIG. 2. (a) T dependence of the R_s at different B. The dashed line represents a fit to EMT, and the fitted T_c is shown in (b) as a black star. (b) B dependence of T_c, extracted from (a) with a 50% criterion, except the lowest T_c, which is found by varying the B at $T = 40$ mK. (c) dc measurement of V_{xx} vs I for various T. Arrows indicate the sweep direction. Curves are offset by 2.2 mV. (d) Zero-field T dependence and B dependence at 30 mK (e) of J_c. The black lines are fits to theory, as explained in the main text.

[black symbol in Fig. 2(b)], and extrapolating to $T_c = 0$ K gives a measure of the upper critical field $B_{c2}(0$ K$) \approx 180$ mK. This corresponds to a coherence length of $\xi \approx 40$ nm close to the values found for *c*-LAO/STO [10,39]. Note that the $T_c(B)$ dependence is expected to go to zero T with a vertical tangent [40], which is not observed due to limits of the measurement. Also, the extracted coherence length depends on the definition of T_c and taking the 5% or 95% transition point for T_c results in $\xi(0)$ of 49 and 35 nm, respectively.

Four-terminal finite bias I-V characteristics are presented in Figs. 2(c)–2(e). When increasing the bias current [Fig. 2(c), red trace], the device is initially in the superconducting state and $V_{xx} = 0$ V, but switches abruptly to a resistive state at the critical current I_c. When reversing the sweep direction (blue trace), the sample returns to the superconducting state at the retrapping current $I_r < I_c$. Such hysteretic behavior can be an effect of Joule heating [41,42], however, since the hysteretic behavior is largely unchanged up to 200 mK, this seems unlikely. Alternatively, hysteretic I-V curves are characteristic for an array of Josephson junctions [40,43] in the underdamped regime. For an individual junction of capacitance C and normal-state resistance R_{JJ} the quality factor is $Q = \omega_p R_{\mathrm{JJ}} C$, where ω_p is the plasma frequency, and the underdamped regime $Q \gg 1$ could naturally appear due to the high dielectric constant of STO providing large junction capacitances. In this scenario the multiple switching events to finite resistive states observed at $T > 250$ mK in Fig. 2(c) are consistent with an array containing junctions with varying critical currents.

The temperature dependence of the critical current density $J_c = I_c/W$ is shown in Fig. 2(d). For $T \lesssim 150$ mK, J_c is constant at ${\sim}28$ mA/m and drops steeply to zero at

around 350 mK. The dotted line represents a fit to the Ginzburg-Landau mean-field result $J_c^{\mathrm{GL}} \propto H_c(0)/\lambda(0)[1 - (T/T_c)^2]^{3/2}[1 + (T/T_c)^2]^{1/2}$, which describes the critical current in homogeneous superconducting thin films [44]. Here, $H_c(0)$ and $\lambda(0)$ refer to the low-temperature value of the critical field and the penetration depth. This model does not describe the data adequately and, moreover, taking values $H_c(0) \sim 1000$ Oe and $\lambda(0) \sim 10~\mu$m appropriate for bulk STO [8], the model estimates a low-field critical current density of $\sim 10 \times 10^{10}$ A/m^2. Estimating a superconducting layer thickness of ~ 10 nm [28] for our sample this amounts to a density of 10 A/m, i.e., three orders of magnitude larger than what we measure. The T dependence of the local superfluid density can be obtained from EMT [24] and assuming proportionality to the measured critical current results in the dashed line in Fig. 2(d). The deviation from the data can be attributed to the connectivity of the array not being accounted for in the model. Fitting to the theory for a junction of arbitrary transparency [45,46] and using the BCS result for the temperature dependence of the gap $\Delta(T)$ [18], we find good agreement with the data for an individual metallic weak link in the dirty limit, with $J_{\mathrm{JJ}} = \frac{\pi \Delta(T)}{2e R_{\mathrm{JJ}}} \tanh \frac{\Delta(T)}{2k_B T}$. This fit is shown by the solid line in Fig. 2(d) with $T_c = 379$ mK, close to the value $T_c = 358$ mK found from Fig. 2(a). The difference is within the width of the distribution $\gamma = 24$ mK.

The critical current density as a function of magnetic field is shown in Fig. 2(e). At high B-field values the sample does not reach the superconducting state, however, a clear transition to a higher resistive state is still observed at a distinct current I_c. For an individual uniform rectangular JJ, a magnetic field will cause the measured critical current to oscillate and follow the Fraunhofer pattern $I_c \propto |\sin(\pi \Phi/\Phi_0)/(\pi \Phi/\Phi_0)|$ [40]. For a sample composed of a random array of junctions, the oscillations average out and we expect $J_c(B)$ to follow the approximate envelope $\propto 1/(1 + B/B_0)^\beta$, where $\beta \approx 1$ depends on the junction geometry [47,48] and the characteristic scale B_0 relates to the average junction area $A_0 = \Phi_0/\pi B_0$. As seen in Fig. 2(e), this simple model shows good overall agreement with the data, yielding $\beta = 1.42$ and a junction area of $0.029 \pm 0.002~\mu$m^2.

In addition to the measurements presented in Fig. 2, the temperature dependence of the critical current was measured at finite B. The resulting superconducting phase diagram of the a-LAO/STO interface is shown in Fig. 3 [49].

A key feature of the superconducting phase in STO-based interfaces is the dome-shaped dependence of the critical temperature on electrostatic doping [11], related to the doping dependence of T_c in bulk STO [8,50]. Figure 4(a) shows $R_s(T)$ for various V_{bg} for the a-LAO/STO heterostructure and Fig. 4(b) shows the corresponding $T_c(V_{\mathrm{bg}})$ dome extracted using EMT, which reaches a maximum T_c of 460 mK at optimal doping. This value is larger than what has been reported previously for LAO/STO-based interfaces and very close to the reported transition temperature of bulk conducting STO at optimal doping [8]. At the lowest V_g (highest R_N) the resistance does not fall to zero and T_c cannot be defined for these curves. As seen in Fig. 4(b), the width of the transition γ decreases monotonically across the dome. At low V_{bg} (high R_N) the $R_s(T)$ curves develop multiple steps, which we ascribe to different regions of the sample entering
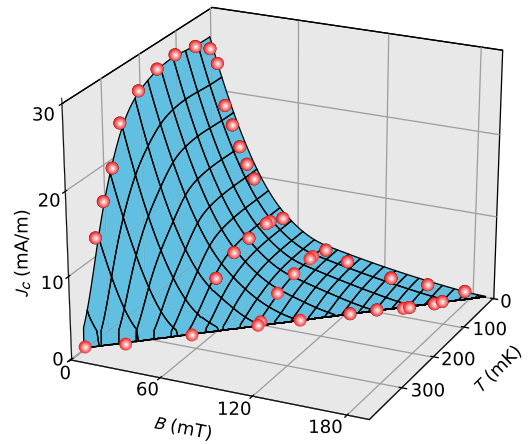

FIG. 3. Full superconducting phase diagram obtained from the dependence of the critical current density on temperature and magnetic field. The surface grid was obtained from interpolation between data points from Figs. 1(b), 2(d), and 2(e) (red). Additional I-V curve measurements at static magnetic fields have been added as well to establish the shape at the interior of the surface. The superconducting region is shaded in blue.

the superconducting state at different temperatures. This is consistent with scanning probe measurements [12], which report a pronounced spatial inhomogeneity in the diamagnetic screening on the underdoped side of the dome.

Further insight into the superconducting phase emerges by comparing the back-gate dependence of the critical current and critical temperature. Figures 5(a) and 5(b) show the I-V characteristics at various V_{bg} obtained in a separate cooldown. At each back-gate voltage, dc current-biased I-V curves and $\partial V/\partial I_{sd}$ were simultaneously measured, from which $I_c(V_{\mathrm{bg}})$ is extracted. The gate dependence of the T_c was obtained using a temperature feedback loop keeping R_s at 50% of the normal-state resistance.

Figure 5(c) shows $I_c(V_{\mathrm{bg}})$ and $T_c(V_{\mathrm{bg}})$ with respect to R_N to compensate for gate hysteresis. Both T_c and I_c exhibit dome-shaped dependencies on doping, however, the two domes peak at significantly different doping levels. Two regimes can be identified: i (for $R_N \lesssim 1.4$ kΩ/sq) and ii (for $\gtrsim 1.4$ kΩ/sq). In regime i the device is on the overdoped side of the dome and T_c increases with R_N. The critical current $I_c(R_N)$ qualitatively follows $T_c(R_N)$ and both exhibit an increase with R_N with a decreasing rate. At $R_N \approx 1.4$ kΩ/sq the critical current peaks
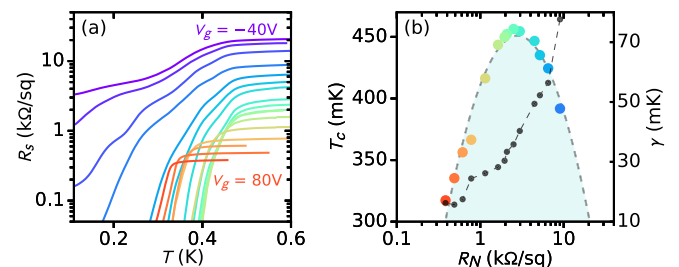

FIG. 4. (a) Dependence of the sheet resistance R_s on temperature for varying back-gate voltages. (b) The critical temperature T_c and width of the transition γ extracted from the curves in (a) using effective medium theory.
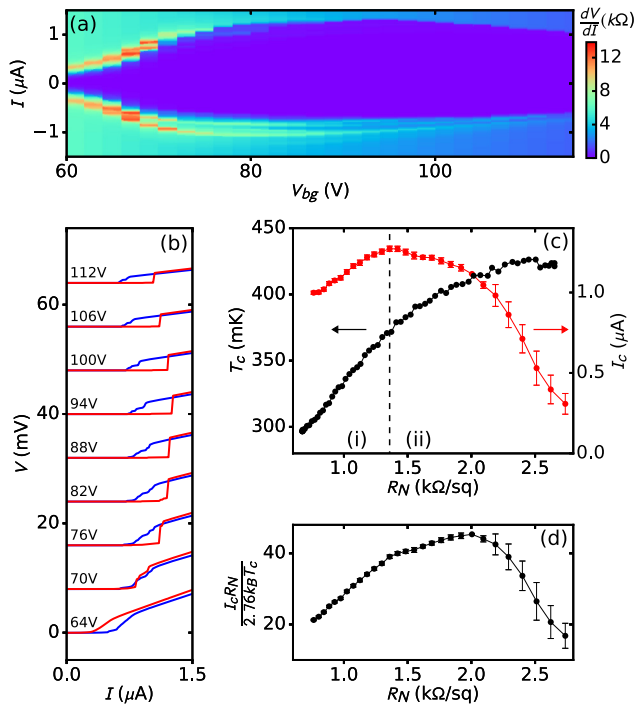
FIG. 5. (a) ac differential resistance measured in a separate cooldown for varying dc bias current (from negative to positive values) and back-gate voltages. (b) Simultaneously measured dc *I*-*V* characteristics for varying back-gate voltages, plotted with a horizontal offset of 5 mV between curves. The bias current is increased in the positive (negative) direction for the red (blue) curve. (c) The critical temperature T_c (black) and the measured critical current I_c (red), extracted from the *I*-*V* characteristics in (b), vs the normal-state resistance R_N (black). (d) The corresponding $I_c R_N$ product. Error bars in (c) and (d) depict the width of the switching region in the *I*-*V* characteristics shown in (b).

at ~ 1.3 μA and in regime *ii*, I_c decreases with R_N while T_c continues to increases until it peaks at $R_N \approx 2.5$ kΩ/sq.

For a conventional homogeneous thin-film superconductor, I_c is described with Ginzburg-Landau theory by $I_c^{\mathrm{GL}} \propto \Delta \propto T_c$ and is expected to follow T_c, unlike the experiment. In the alternative scenario of a Josephson-coupled array, as a simplest model, a single Josephson junction in the superconducting percolation path triggers the transition from the superconducting to the resistive state. The low-temperature critical current is in this case $I_c^{\mathrm{JJ}} \propto \Delta/e R_{\mathrm{JJ}}$, with e being the electron charge and we assume that R_{JJ} depends on electrostatic doping qualitatively similar to R_N. Thus on the overdoped side of the T_c dome, since V_g tunes both T_c and R_N, the Josephson-array scenario allows for a situation where an increase in T_c is accompanied by a decrease of I_c as observed in regime *ii*. Here, I_c is progressively suppressed as R_N increases and domains are decoupled, while T_c does not depend on the coupling between domains but rather on the carrier density of the individual domains. Therefore this behavior provides a qualitative distinction between the homogeneous thin-film and Josephson-array scenarios, and shows that the latter describes the *a*-LAO/STO interface superconductivity. The formation of superconducting weak links is also described as the onset of

"weak superconductivity" and is related to the formation of a pseudogap, shown to occur in the normal state of LAO/STO and high-T_c superconductors [18,51]. Note that the scaling analysis shown in previous work [11,24,26] to capture $T_c(V_{\mathrm{bg}})$ close to the phase transition is also expected to be valid for the transition in a JJA driven by a coupling constant [52].

The *I*-*V* curves shown in Fig. 5(b) exhibit an increasing amount of switching events and a decreasing amount of hysteresis with lowering V_{bg}. This behavior is also consistent with a JJA, in the case of a dominating contribution to the *Q* factors from lowering of the mutual capacitance as the superconducting domains are progressively decoupled and the distribution of critical currents is broadened. For an individual JJ, $I_c R_{\mathrm{JJ}} \propto \Delta$ is a constant, and correspondingly for a regular $N \times N$ array [43], $I_c R_N^{\mathrm{array}} \approx N \frac{\pi}{2} \Delta/e \approx N \frac{\pi}{2} 1.76 k_B T_c/e$ is also expected to be constant for a static array. Using the measured T_c, equal to the average $\bar{T}_c$ of the distribution according to EMT and assuming $R_N = R_N^{\mathrm{array}}$, Fig. 5(d) shows the extracted N as a function of doping which follows a domelike structure peaked at $R_N \approx 1.6$ kΩ/sq intermediate between the center values of $I_c(R_N)$ and $T_c(R_N)$. The varying N suggests a gate-dependent structure of the array, possibly related to the doping dependence of the spatial variations observed in scanning probe experiments [16,17]. The origin of the reversed hysteresis that was reproducibly observed in the I-V curves at lowest V_{bg} remains unknown.

In conclusion, we have demonstrated superconductivity in patterned *a*-LAO/STO and established the superconducting phase diagram. The room-temperature grown top layer enhances the feasibility of conventional micro fabrications techniques for designing gateable mesoscopic superconducting oxide devices. The characteristics of the phase diagram are qualitatively consistent with previous studies of *c*-LAO/STO samples. We recover the domelike dependence of the critical temperature on back-gate voltage with a peak value of 460 mK, significantly larger than observed for the *c*-LAO/STO system and close to the value for bulk conducting STO at optimal doping. From the critical current phase diagram, the observation of multiple resistance steps in the *I*-*V* characteristics and the observation of a pronounced shift between the $T_c(V_{\mathrm{bg}})$ and $I_c(V_{\mathrm{bg}})$ domes, we show that the system can be consistently described by a model of an intrinsic Josephson junction array formed by a random network of weakly coupled superconducting domains. The inhomogeneity could be related to inhomogeneous carrier doping by oxygen vacancies or the tetragonal domain boundaries in the STO crystal. The results highlight the important role of inhomogeneity for the properties of superconductivity in STO-based heterostructures.

[1] B. Josephson, Phys. Lett. **1**, 251 (1962).

[2] A. Y. Kitaev, Phys. Usp. **44**, 131 (2001).

[3] P. Recher, E. V. Sukhorukov, and D. Loss, Phys. Rev. B **63**, 165314 (2001).

[4] Y. Doh, J. van Dam, A. Roest, E. Bakkers, L. Kouwenhoven, and S. De Franceschi, Science **309**, 272 (2005).

[5] L. Hofstetter, S. Csonka, J. Nygard, and C. Schoenenberger, Nature (London) **461**, 960 (2009).

[6] V. Mourik, K. Zuo, S. M. Frolov, S. R. Plissard, E. P. A. M. Bakkers, and L. P. Kouwenhoven, Science **336**, 1003 (2012).

[7] P. Fleury, J. Scott, and J. Worlock, Phys. Rev. Lett. **21**, 16 (1968).

[8] J. Schooley, W. Hosler, E. Ambler, J. Becker, M. Cohen, and C. Koonce, Phys. Rev. Lett. **14**, 305 (1965).

[9] A. Ohtomo and H. Hwang, Nature (London) **427**, 423 (2004).

[10] N. Reyren, S. Thiel, A. D. Caviglia, L. F. Kourkoutis, G. Hammerl, C. Richter, C. W. Schneider, T. Kopp, A.-S. Ruetschi, D. Jaccard, M. Gabay, D. A. Muller, J.-M. Triscone, and J. Mannhart, Science **317**, 1196 (2007).

[11] A. D. Caviglia, S. Gariglio, N. Reyren, D. Jaccard, T. Schneider, M. Gabay, S. Thiel, G. Hammerl, J. Mannhart, and J. M. Triscone, Nature (London) **456**, 624 (2008).

[12] J. A. Bert, K. C. Nowack, B. Kalisky, H. Noad, J. R. Kirtley, C. Bell, H. K. Sato, M. Hosoda, Y. Hikita, H. Y. Hwang, and K. A. Moler, Phys. Rev. B **86**, 060503 (2012).

[13] L. Li, C. Richter, J. Mannhart, and R. Ashoori, Nat. Phys. **7**, 762 (2011).

[14] A. D. Caviglia, M. Gabay, S. Gariglio, N. Reyren, C. Cancellieri, and J. M. Triscone, Phys. Rev. Lett. **104**, 126803 (2010).

[15] L. Fidkowski, H.-C. Jiang, R. M. Lutchyn, and C. Nayak, Phys. Rev. B **87**, 014436 (2013).

[16] B. Kalisky, E. M. Spanton, H. Noad, J. R. Kirtley, K. C. Nowack, C. Bell, H. K. Sato, M. Hosoda, Y. Xie, Y. Hikita, C. Woltmann, G. Pfanzelt, R. Jany, C. Richter, H. Y. Hwang, J. Mannhart, and K. A. Moler, Nat. Mater. **12**, 1091 (2013).

[17] M. Honig, J. Sulpizio, J.Drori, A. Joshua, E. Zeldov, and S. Ilani, Nat. Mater. **12**, 1112 (2013).

[18] C. Richter, H. Boschker, W. Dietsche, E. Fillis-Tsirakis, R. Jany, F. Loder, L. F. Kourkoutis, D. A. Muller, J. R. Kirtley, C. W. Schneider, and J. Mannhart, Nature (London) **502**, 528 (2013).

[19] D. Bucheli, S. Caprara, and M. Grilli, Supercond. Sci. Technol. **28**, 045004 (2015).

[20] E. Fillis-Tsirakis, C. Richter, J. Mannhart, and H. Boschker, New J. Phys. **18** 013046 (2016).

[21] V. L. Berezinskii, Sov. Phys. JETP **32**, 493 (1971).

[22] J. Kosterlitz and D. Thouless, J. Phys. C **6**, 1181 (1973).

[23] M. R. Beasley, J. E. Mooij, and T. P. Orlando, Phys. Rev. Lett. **42**, 1165 (1979).

[24] S. Caprara, J. Biscaras, N. Bergeal, D. Bucheli, S. Hurand, C. Feuillet-Palma, A. Rastogi, R. C. Budhani, J. Lesueur, and M. Grilli, Phys. Rev. B **88**, 020504 (2013).

[25] S. Caprara, M. Grilli, L. Benfatto, and C. Castellani, Phys. Rev. B **84**, 014514 (2011).

[26] J. Biscaras, N. Bergeal, S. Hurand, C. Feuillet-Palma, A. Rastogi, R. C. Budhani, M. Grilli, S. Caprara, and J. Lesueur, Nat. Mater. **12**, 542 (2013).

[27] Z. Q. Liu, C. J. Li, W. M. Lu, X. H. Huang, Z. Huang, S. W. Zeng, X. P. Qiu, L. S. Huang, A. Annadi, J. S. Chen, J. M. D. Coey, T. Venkatesan, and Ariando, Phys. Rev. X **3**, 021010 (2013).

[28] Y. Chen, N. Pryds, J. E. Kleibeuker, G. Koster, J. Sun, E. Stamate, B. Shen, G. Rijnders, and S. Linderoth, Nano Lett. **11**, 3774 (2011).

[29] D. Fuchs, R. Schafer, A. Sleem, R. Schneider, R. Thelen, and H. von Lohneysen, Appl. Phys. Lett. **105** 092602 (2014).

[30] M. Mehta, D. Dikin, C. Bark, S. Ryu, C. Folkman, C. Eom, and V. Chandrasekhar, Nat. Commun. **3**, 955 (2012).

[31] H. S. J. van der Zant, B. J. van Wees, C. J. Muller, H. A. Rijken, and J. E. Mooij, Jpn. J. Appl. Phys. **26**, S3 (1987).

[32] P. Gallagher, M. Lee, J. Williams, and D. Goldhaber-Gordon, Nat. Phys. **10**, 748 (2014).

[33] F. Trier, G. E. D. K. Prawiroatmodjo, M. von Soosten, D. Christensen, T. S. Jespersen, Y. Chen, and N. Pryds, Appl. Phys. Lett. **107**, 191604 (2015).

[34] Y. Z. Chen, F. Trier, T. Wijnands, R. J. Green, N. Gauquelin, R. Egoavil, D. Christensen, G. Koster, M. Huijben, N. Bovet, S. Macke, F. He, R. Sutarto, N. H. Andersen, J. Sulpizio, M. Honig, G. E. D. K. Prawiroatmodjo, T. S. Jespersen, S. Linderoth, S. Ilani, J. Verbeeck, G. Van Tenderloo, G. Rijnders, G. A. Sawatzky, and N. Pryds, Nat. Mater. **14**, 801 (2015).

[35] M. Huijben, G. Rijnders, D. Blank, S. Bals, S. Van Aert, J. Verbeeck, G. Van Tendeloo, A. Brinkman, and H. Hilgenkamp, Nat. Mater. **5**, 556 (2006).

[36] Y. Z. Chen, N. Bovet, T. Kasama, W. W. Gao, S. Yazdi, C. Ma, N. Pryds, and S. Linderoth, Adv. Mater. **26**, 1462 (2014).

[37] J. A. Bert, B. Kalisky, C. Bell, M. Kim, Y. Hikita, H. Y. Hwang, and K. A. Moler, Nat. Phys. **7**, 767 (2011).

[38] The model does not capture the difference in sharpness of the transition close to R_N and $0\,\Omega$ which could be related to a nonsymmetric T_c distribution or phase fluctuations between the islands.

[39] M. Ben Shalom, M. Sachs, D. Rakhmilevitch, A. Palevski, and Y. Dagan, Phys. Rev. Lett. **104**, 126802 (2010).

[40] M. Tinkham, *Introduction to Superconductivity* (McGraw-Hill, New York, 1996).

[41] M. Tinkham, J. U. Free, C. N. Lau, and N. Markovic, Phys. Rev. B **68**, 134515 (2003).

[42] H. Courtois, M. Meschke, J. T. Peltonen, and J. P. Pekola, Phys. Rev. Lett. **101**, 067002 (2008).

[43] W. Yu and D. Stroud, Phys. Rev. B **46**, 14005 (1992).

[44] W. Skocpol, M. Beasley, and M. Tinkham, J. Appl. Phys. **45**, 4054 (1974).

[45] I. O. Kulik and A. O. Omelyanchuk, JETP Lett. **21**, 96 (1975).

[46] W. Haberkorn, H. Knauer, and J. Richter, Phys. Status Solidi A **47**, K161 (1978).

[47] D. van der Laan, H. van Eck, B. ten Haken, J. Schwartz, and H. ten Kate, IEEE Trans. Appl. Supercond. **11**, 3345 (2001).

[48] K. Mueller, D. Matthews, and R. Driver, Physica C **191**, 339 (1992).

[49] To obtain the 3D surface grid, the J_c data points obtained from the I-V curves were fitted to theory and smoothed using a Hanning window and connected by interpolation.

[50] X. Lin, G. Bridoux, A. Gourgout, G. Seyfarth, S. Kramer, M. Nardone, B. Fauque, and K. Behnia, Phys. Rev. Lett. **112**, 207002 (2014).

[51] E. Talantsev and J. Tallon, Nat. Commun. **6**, 7820 (2015).

[52] S. Sondhi, S. M. Girvin, J. P. Carini, and D. Shahar, Rev. Mod. Phys. **69** 315 (1997).